Photoinduced pure spin-current injection in graphene with Rashba spin-orbit interaction

Julien Rioux and Guido Burkard
Department of Physics, University of Konstanz, D-78457 Konstanz, Germany
(Received 27 May 2014; revised manuscript received 14 July 2014; published 28 July 2014)

We propose a photoexcitation scheme for pure spin-current generation in graphene subject to a Rashba spin-orbit coupling. Although excitation using circularly polarized light does not result in optical orientation of spins in graphene unless an additional magnetic field is present, we show that excitation with linearly polarized light at normal incidence yields spin-current injection without magnetic field. Spins are polarized within the graphene plane and are displaced in opposite directions, with no net charge displacement. The direction of the spin current is determined by the linear polarization axis of the light, and the injection rate is proportional to the intensity. The technique is tunable via an applied bias voltage and is accessible over a wide frequency range. We predict a spin-current polarization as high as 75% for photon frequencies comparable to the Rashba frequency. Spin-current injection via optical methods removes the need for ferromagnetic contacts, which have been identified as a possible source of spin scattering in electrical spin injection in graphene.

DOI: 10.1103/PhysRevB.90.035210 PACS number(s): 72.25.Fe, 73.50.Pz, 78.67.Wj

I. INTRODUCTION

The isolation of graphene, a single layer of graphite, has opened the door to research on atomically thin crystals with Dirac-like electrons [1]. In addition to the high mobility of charge carriers in graphene, rendering it attractive for use in electronics, long spin relaxation times are expected due to the spinless atomic nucleus of ^{12}C and the small spin-orbit coupling, further promoting graphene as an interesting material for spintronics applications [2,3].

The first studies of spin injection in graphene have reported a diffusive spin current injected via ferromagnetic contacts, initially in a two-terminal geometry [4] and soon after in a nonlocal four-terminal geometry [5–7]. The technique is improved when inserting MgO as an insulating tunnel barrier [8] and achieves up to 60% spin polarization when using a second layer of graphene as the tunnel barrier [9]. Thus far, the obtained spin lifetimes are low compared to expectations, and the ferromagnetic contacts remain a possible source of spin scattering explaining this discrepancy [10]. The efforts towards electrical spin injection in graphene are reviewed by Shiraishi [11]. Others have reported spin-current injection in graphene using dynamical [12,13] and thermal [14,15] methods.

Optical orientation is another means of injecting spin-polarized carriers into semiconductors exhibiting spin-orbit coupling [16]. Spin photocurrents resulting from absorption of linearly polarized light have been proposed and demonstrated in GaAs quantum wells [17–20]. Although graphene spintronics offers very interesting prospects, the optical injection and control of spin currents in graphene have yet to be investigated. Optical methods are motivated by the relatively strong 2.3% absorption of light by a single graphene sheet over a wide range of frequencies [21]. Since light interacts with the orbital degree of freedom, any optical manipulation of the spin degree of freedom relies on the presence of coupling between these two degrees of freedom. Graphene's weak spin-orbit interaction (SOI), which limits the application range for spin photoinjection and, conversely, for spin readout by optical methods [22], is increased through heavy-atom intercalation [23], impurities [24], or hydrogenation [25,26]. In contrast to intrinsic SOI, Rashba-type SOI is tunable and can be increased to a strength sufficiently large that optical spin injection in graphene with an in-plane magnetic field has recently been proposed [27].

In this paper, optical spin-current injection is investigated in graphene subject to a Rashba spin-orbit coupling. Due to the chirality of graphene electrons and the nature of the optical matrix element, we show that photoexcitation results in the injection of a pure spin current, without accompanying charge current. We thus predict spin-current injection in graphene via optical methods without contacts, eliminating a possible source of spin scattering. The paper is organized as follows. The effective Hamiltonian and matrix elements used for the calculations are presented in Sec. II. Spin-current injection and its polarization are calculated in Sec. III. We summarize and discuss our results in Sec. IV.

II. HAMILTONIAN AND MATRIX ELEMENTS

Band electrons in single-layer graphene are described by the usual Dirac Hamiltonian in the linear dispersion regime [28],

$$H_0 = \hbar v_F(\tau\sigma_x k_x + \sigma_y k_y), \tag{1}$$

where v_F is the Fermi velocity, $\boldsymbol{\sigma}$ are the Pauli matrices, here acting on graphene's A and B sublattice space, and $\mathbf{k}$ is the in-plane crystal momentum relative to the K point ($\tau = 1$) or the K' point ($\tau = -1$). An external out-of-plane electric field breaks inversion symmetry and introduces the Rashba spin-orbit coupling term

$$H_R = \hbar\Omega_R(\tau\sigma_x S_y - \sigma_y S_x), \tag{2}$$

where Ω_R is the Rashba frequency and $\mathbf{S}$ is the electron spin [28]. This can be induced by the substrate or by additional gates generating a voltage gradient perpendicular to the sample. The result of diagonalizing $H_0 + H_R$ yields four energy bands with an isotropic band dispersion quadratic in k for $k \ll \Omega_R/2v_F$ and linear in k for $k \gg \Omega_R/v_F$, shown in Fig. 1(a). The lowest-energy conduction band c_1 and highest-energy valence band v_2 are degenerate at the K point, and so-called "split-off" conduction band c_2 and valence band v_1 are respectively shifted up and down by an energy $\hbar\Omega_R$

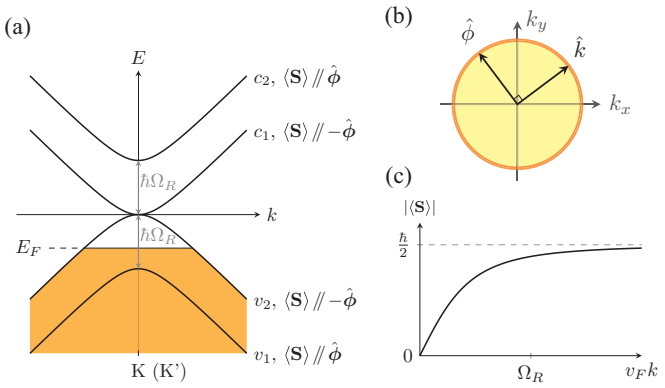

FIG. 1. (Color online) (a) Energy-momentum dispersion of graphene with Rashba spin-orbit coupling; (b) vectors defining the orientation in the graphene plane; and (c) magnitude of the spin expectation value as a function of crystal momentum.

from the charge neutrality point [29]. In the two gapless bands the expectation value of the electron spin $\langle \mathbf{S} \rangle$ is oriented antiparallel with $\hat{\phi} = \hat{z} \times \hat{k}$, where $\hat{k}$ is the unit vector parallel to the direction of $\mathbf{k}$ [cf. Fig. 1(b)] and $\hat{z}$ is normal to the graphene plane, while $\langle \mathbf{S} \rangle$ is oriented parallel with $\hat{\phi}$ for the split-off bands. In all cases, the expectation value of spin has a magnitude

$$|\langle \mathbf{S} \rangle| = \frac{v_F \hbar k}{\sqrt{\Omega_R^2 + 4 v_F^2 k^2}}, \tag{3}$$

shown in Fig. 1(c), reaching $\hbar/2$ for large $k \gg \Omega_R / v_F$.

The interaction of the material with an external vector potential $\mathbf{A}$ describing an electromagnetic field is treated within minimal coupling by substituting $\hbar\mathbf{k}$ by $\hbar\mathbf{k} - e\mathbf{A}$ in the Hamiltonian. The linear response under photoexcitation is readily obtained from the matrix elements, between initial and final states, of the $\mathbf{A} \cdot \mathbf{v}$ interaction term appearing in minimal coupling. Matrix elements of the velocity operator $\mathbf{v} = \boldsymbol{\sigma} v_F$ and of the spin operator are given in the Appendix.

III. SPIN-CURRENT INJECTION IN GRAPHENE

In this section, we consider photoexcitation of a graphene layer with Rashba SOI under a monochromatic electric field

$$\mathbf{E}(t) = \mathbf{E}(\omega) e^{-i\omega t} + \mathbf{E}^*(\omega) e^{i\omega t}. \tag{4}$$

The $\mathbf{k}$-dependent spin polarization of the eigenstates [cf. Eq. (3)] is exploited to inject photoinduced spin currents. The spin textures in the K and K' valleys are exactly the same, thus carriers of momentum $\mathbf{k}$ near K and K' are excited with equal spin polarization. Moreover, carriers at $-\mathbf{k}$ are excited with opposite spin polarization, resulting in a pure spin current at normal incidence.

We use the generally accepted symmetrized spin-current operator $\mathbf{J}_s = \frac{1}{2}(\mathbf{vS} + \mathbf{Sv})$ [30], where juxtaposed vectors form the dyadic product. The injection rate $\dot{\mathbf{J}}_s$ is derived by solving the Heisenberg equation of motion and keeping the nonzero term at lowest order in the field. The resulting spin-current injection rate is linear in intensity and is written in component notation [19,31]

$$\dot{J}_s^{ab} = \mu_1^{abcd}(\omega) E^{c*}(\omega) E^d(\omega), \tag{5}$$

where Roman superscripts indicate Cartesian components and repeated superscripts are summed over. The response pseudotensor $\mu_1^{abcd}(\omega)$, derived at a level equivalent to Fermi's golden rule and including both contributions of electrons and holes, is

$$\mu_1^{abcd}(\omega) = \frac{2\pi e^2}{\hbar^2 \omega^2} \sum_{cv} \int \frac{d^2k}{4\pi^2} \left[(J_s)_{cc}^{ab} - (J_s)_{vv}^{ab} \right] \times v_{cv}^{c*}(\mathbf{k}) v_{cv}^{d}(\mathbf{k}) \, \delta[\omega_{cv}(\mathbf{k}) - \omega], \tag{6}$$

where

$$(J_s)_{cc}^{ab}(\mathbf{k}) \equiv \sum_m \frac{1}{2} \left[v_{cm}^a(\mathbf{k}) S_{mc}^b(\mathbf{k}) + S_{cm}^a(\mathbf{k}) v_{mc}^b(\mathbf{k}) \right] \tag{7}$$

is the diagonal matrix element of the spin-current operator, $\mathbf{v}_{mn}(\mathbf{k})$ and $\mathbf{S}_{mn}(\mathbf{k})$ indicate matrix elements of, respectively, the velocity and spin operators, and $\omega_{cv}(\mathbf{k}) \equiv [E_c(\mathbf{k}) - E_v(\mathbf{k})]/\hbar$ is the energy difference between conduction and valence bands; the sum over m includes all band indices, while the sum over c (v) includes conduction (valence) bands only. Within the Dirac model of Sec. II, only one independent nonzero component exists: $\mu_1^{xyxx}(\omega)$. There are in total eight nonzero components, related by

$$\mu_1^{xyxx} = \mu_1^{yxxx} = \mu_1^{yxxy} = \mu_1^{yyyx} = -\mu_1^{xxxy} = -\mu_1^{xxyx} = -\mu_1^{xyyy} = -\mu_1^{yxyy}. \tag{8}$$

Evaluating the charge current injection in the same approach yields a vanishing response tensor η_1 [19], thus the spin current presented here is pure, without accompanying charge current.

A general oscillatory electric field for a normally incident wave has the form $\mathbf{E}(\omega) = E_\omega e^{i\varphi_\omega} (\hat{\mathbf{x}}_\omega + \hat{\mathbf{y}}_\omega e^{i\delta\varphi_\omega})/\sqrt{2}$, where the amplitude E_ω and the phase parameters φ_ω and $\delta\varphi_\omega$ are chosen to be real for an appropriate choice of orthonormal vectors $\hat{\mathbf{x}}_\omega$ and $\hat{\mathbf{y}}_\omega$ in the graphene plane. From Eq. (5) and the symmetry of $\mu_1^{abcd}(\omega)$ given above, the injection rate of the spin current is given by the general dyadic expression

$$\dot{\mathbf{J}}_s = \mu_1^{xyxx}(\omega) |E_\omega|^2 \cos(\delta\varphi_\omega) (\hat{\mathbf{y}}_\omega \hat{\mathbf{y}}_\omega - \hat{\mathbf{x}}_\omega \hat{\mathbf{x}}_\omega). \tag{9}$$

Due to the cosine dependence on the Stokes parameter $\delta\varphi_\omega$, the spin-current injection is zero for circularly polarized light ($\delta\varphi_\omega = \pm\frac{\pi}{2}$) and maximum for linearly polarized light ($\delta\varphi_\omega = 0$), in which latter case we obtain

$$\dot{\mathbf{J}}_s = \mu_1^{xyxx}(\omega) |E_\omega|^2 (\hat{\mathbf{e}}_\omega \hat{\mathbf{e}}_\omega^\perp + \hat{\mathbf{e}}_\omega^\perp \hat{\mathbf{e}}_\omega), \tag{10}$$

where $\hat{\mathbf{e}}_\omega \equiv (\hat{\mathbf{x}}_\omega + \hat{\mathbf{y}}_\omega)/\sqrt{2}$ is the linear polarization axis and $\hat{\mathbf{e}}_\omega^\perp = \hat{\mathbf{z}} \times \hat{\mathbf{e}}_\omega$ is an in-plane unit vector perpendicular to the polarization axis. Equation (10) is the main result of this paper. Linearly polarized light induces a spin-current injection proportional to the intensity, with the direction determined by the polarization axis. Within the isotropic model presented here, the magnitude of the current is insensitive to rotation of the crystal axes with respect to the normal.

The single independent component $\mu_1^{xyxx}(\omega)$ of the injection tensor gives the magnitude of the resulting current. We

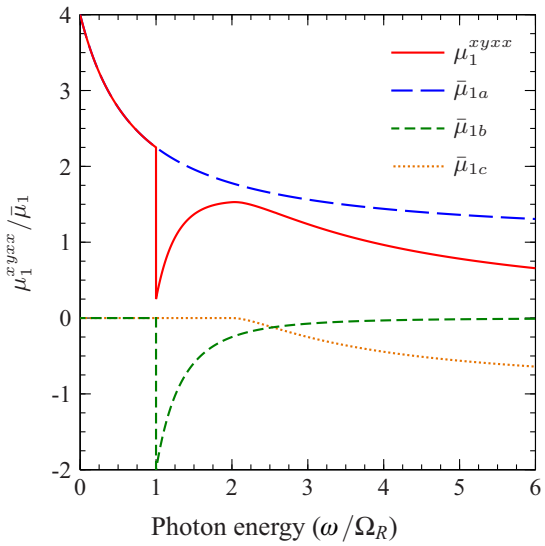

FIG. 2. (Color online) Spin-current injection strength for graphene with Rashba spin-orbit interaction. The single independent component $\mu_1^{xyxx}(\omega)$ of the total spin-current injection tensor [Eq. (11)], as well as the individual contributions $\bar{\mu}_{1a-c}(\omega)$ [Eq. (12)], are shown as a function of the light frequency ω for the case of intrinsic graphene ($E_F = 0$).

find that it is built up from three contributions,

$$\mu_1^{xyxx}(\omega) = \bar{\mu}_{1a}(\omega)\,\Theta(\omega-\omega_F) + \tfrac{1}{2}\bar{\mu}_{1b}(\omega)[\Theta(\omega-\omega_F-\Omega_R) + \Theta(\omega-\omega_F+\Omega_R)] + \bar{\mu}_{1c}(\omega)\,\Theta(\omega-\omega_F), \quad (11)$$

where $\hbar\omega_F \equiv 2\,|E_F|$ is twice the Fermi level and $\Theta(x)$ is the Heaviside step function. The three contributions $\bar{\mu}_{1a-c}(\omega)$ correspond, in order, to contributions arising from the following band-to-band transitions [cf. Fig. 1(a)]: (a) from v_2 to c_1, (b) from v_2 to c_2 and from v_1 to c_1 with equal contribution, and (c) from v_1 to c_2. They are given by

$$\bar{\mu}_{1a}(\omega) = \bar{\mu}_1(\omega)\frac{(\omega+2\Omega_R)^2}{(\omega+\Omega_R)^2}, \quad (12a)$$

$$\bar{\mu}_{1b}(\omega) = -2\bar{\mu}_1(\omega)\frac{\Omega_R^3}{\omega^3}\Theta(\omega-\Omega_R), \quad (12b)$$

$$\bar{\mu}_{1c}(\omega) = -\bar{\mu}_1(\omega)\frac{(\omega-2\Omega_R)^2}{(\omega-\Omega_R)^2}\Theta(\omega-2\Omega_R), \quad (12c)$$

where $\bar{\mu}_1(\omega) \equiv e^2 v_F\,(16\hbar\omega)^{-1}$ including the valley degeneracy. The individual contributions $\bar{\mu}_{1a-c}(\omega)$ and the total spin-current injection tensor for intrinsic graphene are plotted as a function of the light frequency in Fig. 2.

At photon energy less than the Rashba frequency, only $\bar{\mu}_{1a}$ arising from the low-energy bands contributes to the total spin-current injection, as transitions involving other bands are energetically forbidden. This contribution is maximal in the limit $\omega \to 0$, decreases monotonically with frequency, and mostly dictates the total spin-current injection everywhere except near the onset at $\omega = \Omega_R$ and in the $\omega \gg \Omega_R$ limit. At photon energy equal to the Rashba frequency, $\omega = \Omega_R$, transitions involving one split-off band start contributing. This contribution, $\bar{\mu}_{1b}$, opposes the previous contribution, $\bar{\mu}_{1a}$, and has a sharp onset where the two contributions are roughly of the same amplitude, resulting in a sharp dip in the total spin-current injection. However, $\bar{\mu}_{1b}$ decreases to zero fairly quickly with increasing frequency, and $\bar{\mu}_{1a}$ is again the dominant contribution. Another onset occurs at $\omega = 2\Omega_R$, where transitions from the split-off valence to the split-off conduction band start occurring. This contribution, $\bar{\mu}_{1c}$, is initially small, increases with increasing frequency, and opposes the initial contribution, $\bar{\mu}_{1a}$. At photon energy much larger than the Rashba frequency, $\omega \gg \Omega_R$, the contributions $\bar{\mu}_{1a}$ and $\bar{\mu}_{1c}$ tend to $\bar{\mu}_1$ and $-\bar{\mu}_1$, respectively, and the overall spin-current injection is zero.

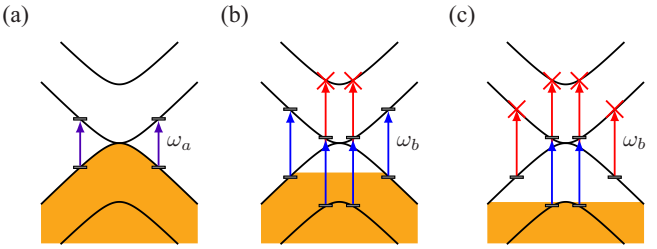

FIG. 3. (Color online) Photoinduced pure spin-current injection schemes. (a) Intrinsic graphene at low energy, $\omega_a < \Omega_R$, yields the strongest spin-current injection. (b) For midrange energy, $\Omega_R < \omega_b < 2\Omega_R$, the spin-current injection strength improves by tuning the Fermi level to $|E_F| = \frac{1}{2}\hbar\Omega_R$ to Pauli block half of the transitions involving a split-off band. (c) For the same frequency range, further increasing the Fermi level to $|E_F| = \hbar\Omega_R$ results in the Pauli blocking of transitions involving the gapless bands. This yields a reversal of the spin-current injection.

For intrinsic graphene, the spin-current injection strength $\mu_1^{xyxx}(\omega)$ is positive at all frequencies. The strongest spin-current injection is achieved when $\omega < \Omega_R$, a situation illustrated in Fig. 3(a). The spin-current injection decreases significantly for frequency above $\omega = \Omega_R$, once transitions involving one split-off band start contributing. It is possible to alleviate this effect by tuning the Fermi level E_F away from the charge neutrality point, as in Fig. 3(b). The transition from the lowest valence band is then Pauli blocked, and the diminishing contribution originating from $\bar{\mu}_{1b}$ is reduced. This results in an increased total spin-current injection for frequencies in the range $\omega_F < \omega < \omega_F + \Omega_R$. This Pauli-blocking scheme also scales to higher energies, allowing one to increase the photoexcitation effect in a tunable range of frequencies. The maximal spin-current injection at a given frequency ω is achieved by tuning the Fermi level such that $E_F = (2\hbar\omega - \hbar\Omega_R)/4$. Examples of nonzero doping are given in Fig. 4, showing the reduction of the dip in spin-current injection that occurs for intrinsic graphene at $\omega = \Omega_R$ by tuning the Fermi level to $\omega_F = \Omega_R$. For larger values of the Fermi level, when $\omega_F > \Omega_R$, the sign of $\mu_1^{xyxx}(\omega)$ is also affected by the doping, taking negative values for $\omega < \omega_F$ and positive values for $\omega > \omega_F$. This occurs since the positive and usually dominant contribution arising from the gapless bands, $\bar{\mu}_{1a}$, is Pauli blocked for $\omega < \omega_F$, as illustrated in Fig. 3(c). As seen in Fig. 4, the benefits of the Pauli-blocking scheme to increase the spin-current injection strength are really substantial only from $\omega = \Omega_R$ to about $\omega = 3\Omega_R$.

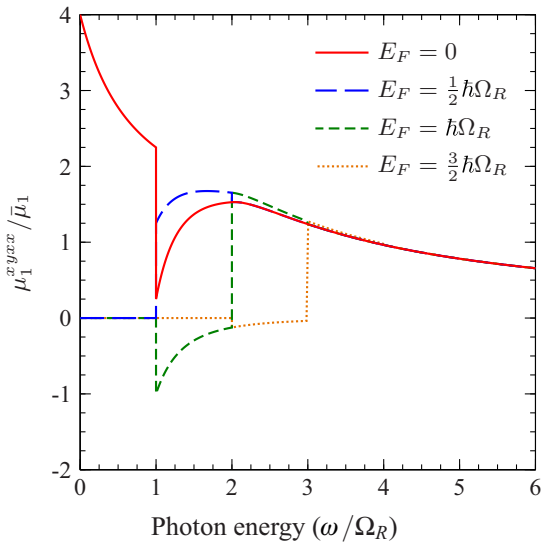

FIG. 4. (Color online) Spin-current injection strength $\mu_1^{xyxx}(\omega)$ for graphene with Rashba spin-orbit interaction [Eq. (11)] for varying values of the Fermi level ($E_F = 0, \frac{1}{2}\hbar\Omega_R, \hbar\Omega_R, \frac{3}{2}\hbar\Omega_R$).

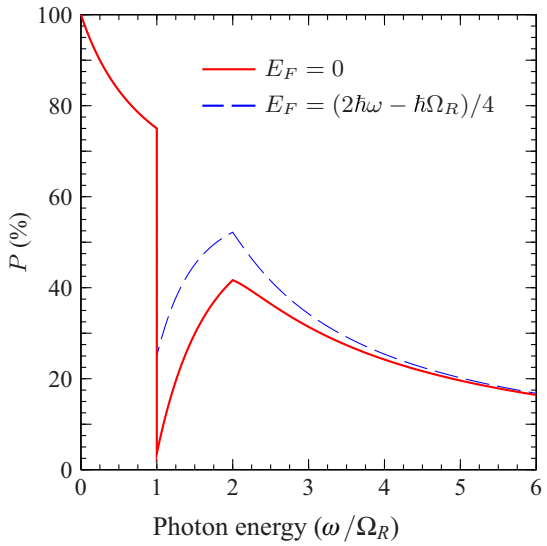

FIG. 5. (Color online) Spin-current polarization per carrier, P, for graphene with Rashba spin-orbit interaction [Eq. (15)] for intrinsic graphene ($E_F = 0$) and for the maximal case making use of Pauli blocking [$E_F = (2\hbar\omega - \hbar\Omega_R)/4$].

A measure of the polarization P of the injected spin current is obtained by taking the ratio of the injection rates between spin-current injection and carrier injection, and normalizing by the maximal velocity v_F and spin $\hbar/2$ for the carriers. Just as the spin-current injection rate, Eq. (5), the injection rate for the density of conduction electrons is proportional to the light intensity and is written as

$$\dot{n} = \xi_1^{ab}(\omega) E^{a*}(\omega) E^b(\omega). \tag{13}$$

The response tensor $\xi_1^{ab}(\omega)$ is computed using Fermi's golden rule [32], yielding, for the intrinsic graphene Hamiltonian including Rashba spin-orbit coupling,

$$\xi_1^{ab}(\omega) = \frac{\sigma_0 \delta^{ab}}{(\hbar\omega)} \left(\frac{\omega + 2\Omega_R}{\omega + \Omega_R} + 2\frac{\Omega_R^2}{\omega^2}\Theta(\omega - \Omega_R) + \frac{\omega - 2\Omega_R}{\omega - \Omega_R}\Theta(\omega - 2\Omega_R) \right), \tag{14}$$

where σ_0 is the universal optical conductivity of freestanding graphene, $\sigma_0 = e^2/4\hbar$ [21,33].

For linearly polarized light, which yields the maximal spin-current polarization, we have

$$P = \frac{|\dot{\mathbf{J}}_s|}{\frac{\hbar}{2} v_F \dot{n}} = \frac{\left|\mu_1^{xxxy}(\omega)\right|}{\frac{\hbar}{2} v_F \left|\xi_1^{xx}(\omega)\right|}. \tag{15}$$

This measure is plotted as a function of light frequency in Fig. 5, showing the spin-current polarization for intrinsic graphene ($E_F = 0$) and the maximally achievable polarization making use of the Pauli-blocking scheme [$E_F = (2\hbar\omega - \hbar\Omega_R)/4$]. Photoinduced spin-current injection with linearly polarized light yields up to 100% polarization in the limit $\omega \to 0$. The polarization decreases with increasing frequency but remains greater than 75% for $\omega < \Omega_R$. At the onset for transitions involving a split-off band, $\omega = \Omega_R$, the polarization drops sharply to 3.6% (25% in the maximal case) before steadily recovering and reaching 42% (52% in the maximal case) at the next onset, $\omega = 2\Omega_R$. Although the polarization then decreases monotonically, it remains as large as 20% at $\omega = 5\Omega_R$.

IV. SUMMARY

The injection of pure spin currents in graphene with Rashba spin-orbit coupling via photoexcitation has been presented. The spin-current injection strength is zero for circularly polarized light and maximal for linearly polarized light, with the spin-current injection rate given in Eq. (10). The injection rate is proportional to the light intensity and the direction of the current follows the polarization axis. Multiple regimes of excitation have been proposed, covering a wide range of photon frequencies. The technique achieves very high spin-current polarization, above 75% at frequencies below the Rashba frequency, roughly 50% at twice the Rashba frequency, and remains as high as 20% at five times the Rashba frequency. In comparison, electrical injection has recently achieved 60% polarization [9].

The injection of a pure spin current is interesting for spintronics applications, and such currents could be detected via electrical edge currents [28], electrical currents [34], pump-probe spectroscopy [20], or Faraday rotation [35]. Spin-current injection via optical methods removes the need for ferromagnetic contacts, which have been identified as a possible source of spin scattering in electrical spin injection in graphene. Since carriers are injected ballistically with high carrier velocities, on the order of the Fermi velocity, the spin separation can reach a commensurate distance after excitation before the spin current decays, its lifetime limited by momentum relaxation [36]. A careful treatment of the subsequent carrier dynamics after injection, including the effect of disorder, inhomogeneity in doping level, and SOI strength, is of interest and the topic of future work.

The range of frequencies yielding large spin-current polarization is increased by a larger spin-orbit coupling strength. A number of studies have reported enhanced SOI in graphene [23–26]. The optical injection of a spin current in bilayer graphene represents another interesting avenue as it presents a stronger SOI [37]. While the dependence of the magnitude $\mu_1^{xyxx}(\omega)$ as a function of light frequency for bilayer graphene is necessarily more complicated than that of graphene, due to the additional available interband transitions, at the simplest level an isotropic band structure model can be used so that the symmetry considerations of the present paper hold.

In previous proposals of optical spin-current injection in low-dimensional structures, spin displacement results from the interference of absorption pathways for left and right circularly polarized components of the linearly polarized light [17–20]. Due to the completely different band symmetry, such optical orientation of the electron spin under circularly polarized light is not possible in graphene without applying an additional magnetic field [27]. Nevertheless, we have shown that optical pure spin-current injection in graphene is possible, with in-plane spin and velocity components and without a magnetic field.

ACKNOWLEDGMENTS

This work was supported by the Konstanz Center for Applied Photonics (CAP) and by the Deutsche Forschungsgemeinschaft (DFG) through SFB 767.

APPENDIX: MATRIX ELEMENTS

The matrix elements necessary to calculate the spin-current injection tensor $\mu_1^{abcd}(\omega)$ according to Eq. (6) are as follows. The velocity operator $\mathbf{v} = \boldsymbol{\sigma} v_F$, written in the eigenstate basis $\{c_1, v_2, c_2, v_1\}$, takes the form

$$\mathbf{v} = \frac{\Omega_R}{\sqrt{\Omega_R^2 + 4v_F^2 k^2}} \begin{pmatrix} \frac{\hbar k}{m^*} A & v_F B \\ v_F B^\dagger & \frac{\hbar k}{m^*} A \end{pmatrix}, \tag{A1}$$

where

$$A \equiv \begin{pmatrix} \hat{k} & i\tau\hat{\phi} \\ -i\tau\hat{\phi} & -\hat{k} \end{pmatrix}, \tag{A2}$$

$$B \equiv \begin{pmatrix} -i\hat{\phi} & -\tau\hat{k} \\ \tau\hat{k} & i\hat{\phi} \end{pmatrix}, \tag{A3}$$

and $m^* = \hbar\Omega_R/2v_F^2$ is the effective mass describing the quadratic band dispersion of graphene with Rashba SOI in the limit $k \to 0$. The spin operator written in the same eigenstate basis takes the form

$$\mathbf{S} = \frac{\hbar}{2} \frac{1}{\sqrt{\Omega_R^2 + 4v_F^2 k^2}} \begin{pmatrix} -C & D \\ D^\dagger & C \end{pmatrix}, \tag{A4}$$

where

$$C \equiv \begin{pmatrix} 2v_F k\hat{\phi} & -\tau\Omega_R\hat{z} \\ -\tau\Omega_R\hat{z} & 2kv_F\hat{\phi} \end{pmatrix}, \tag{A5}$$

$$D \equiv \begin{pmatrix} 2v_F k\hat{z} + i\sqrt{\Omega_R^2 + 4v_F^2 k^2}\,\hat{k} & \tau\Omega_R\hat{\phi} \\ \tau\Omega_R\hat{\phi} & 2v_F k\hat{z} + i\sqrt{\Omega_R^2 + 4v_F^2 k^2}\,\hat{k} \end{pmatrix}. \tag{A6}$$

From these one can obtain matrix elements of the spin-current operator following Eq. (7).

[1] K. S. Novoselov, A. K. Geim, S. V. Morozov, D. Jiang, Y. Zhang, S. V. Dubonos, I. V. Grigorieva, and A. A. Firsov, Science **306**, 666 (2004).

[2] B. Trauzettel, D. V. Bulaev, D. Loss, and G. Burkard, Nat. Phys. **3**, 192 (2007).

[3] D. S. L. Abergel, V. Apalkov, J. Berashevich, K. Ziegler, and T. Chakraborty, Adv. Phys. **59**, 261 (2010).

[4] E. W. Hill, A. K. Geim, K. Novoselov, F. Schedin, and P. Blake, IEEE Trans. Magn. **42**, 2694 (2006).

[5] M. Ohishi, M. Shiraishi, R. Nouchi, T. Nozaki, T. Shinjo, and Y. Suzuki, Jpn. J. Appl. Phys. **46**, L605 (2007).

[6] N. Tombros, C. Józsa, M. Popinciuc, H. T. Jonkman, and B. J. van Wees, Nature (London) **448**, 571 (2007).

[7] S. Cho, Y.-F. Chen, and M. S. Fuhrer, Appl. Phys. Lett. **91**, 123105 (2007).

[8] W. Han, K. Pi, K. M. McCreary, Y. Li, J. J. I. Wong, A. G. Swartz, and R. K. Kawakami, Phys. Rev. Lett. **105**, 167202 (2010).

[9] A. L. Friedman, O. M. J. van 't Erve, C. H. Li, J. T. Robinson, and B. T. Jonker, Nat. Commun. **5**, 3161 (2014).

[10] F. Volmer, M. Drögeler, E. Maynicke, N. von den Driesch, M. L. Boschen, G. Güntherodt, and B. Beschoten, Phys. Rev. B **88**, 161405 (2013).

[11] M. Shiraishi, in *Graphene: Properties, Preparation, Characterisation and Devices*, edited by V. Skákalová and A. B. Kaiser (Woodhead Publishing, Cambridge, 2014), Chap. 13, pp. 324–340.

[12] A. K. Patra, S. Singh, B. Barin, Y. Lee, J. H. Ahn, E. del Barco, E. R. Mucciolo, and B. Özyilmaz, Appl. Phys. Lett. **101**, 162407 (2012).

[13] Z. Tang, E. Shikoh, H. Ago, K. Kawahara, Y. Ando, T. Shinjo, and M. Shiraishi, Phys. Rev. B **87**, 140401 (2013).
[14] M. Zeng, Y. Feng, and G. Liang, Nano Lett. **11**, 1369 (2011).
[15] A. Torres, M. P. Lima, A. Fazzio, and A. J. R. da Silva, Appl. Phys. Lett. **104**, 072412 (2014).
[16] M. I. D'yakonov and V. I. Perel', in *Optical Orientation*, edited by F. Meier and B. P. Zakharchenya, Modern Problems in Condensed Matter Sciences Vol. 8 (North-Holland, Amsterdam, 1984), Chap. 2, pp. 15–71.
[17] S. A. Tarasenko and E. L. Ivchenko, Pis'ma Zh. Eksp. Teor. Fiz. **81**, 292 (2005) [JETP Lett. **81**, 231 (2005)].
[18] E. Ya. Sherman, A. Najmaie, and J. E. Sipe, Appl. Phys. Lett. **86**, 122103 (2005).
[19] R. D. R. Bhat, F. Nastos, A. Najmaie, and J. E. Sipe, Phys. Rev. Lett. **94**, 096603 (2005).
[20] H. Zhao, X. Pan, A. L. Smirl, R. D. R. Bhat, A. Najmaie, J. E. Sipe, and H. M. van Driel, Phys. Rev. B **72**, 201302 (2005).
[21] R. R. Nair, P. Blake, A. N. Grigorenko, K. S. Novoselov, T. J. Booth, T. Stauber, N. M. R. Peres, and A. K. Geim, Science **320**, 1308 (2008).
[22] D. A. Pesin and A. H. MacDonald, Nat. Mater. **11**, 409 (2012).
[23] D. Marchenko, A. Varykhalov, M. R. Scholz, G. Bihlmayer, E. I. Rashba, A. Rybkin, A. M. Shikin, and O. Rader, Nat. Commun. **3**, 1232 (2012).
[24] A. H. Castro Neto and F. Guinea, Phys. Rev. Lett. **103**, 026804 (2009).
[25] J. Balakrishnan, G. K. W. Koon, M. Jaiswal, A. H. Castro Neto, and B. Özyilmaz, Nat. Phys. **9**, 284 (2013).
[26] M. Gmitra, D. Kochan, and J. Fabian, Phys. Rev. Lett. **110**, 246602 (2013).
[27] M. Inglot, V. K. Dugaev, E. Ya. Sherman, and J. Barnaś, Phys. Rev. B **89**, 155411 (2014).
[28] C. L. Kane and E. J. Mele, Phys. Rev. Lett. **95**, 226801 (2005).
[29] E. I. Rashba, Phys. Rev. B **79**, 161409 (2009).
[30] E. I. Rashba, Phys. Rev. B **70**, 161201 (2004).
[31] Using the Gaussian system of quantities and cgs units throughout.
[32] J. Rioux, G. Burkard, and J. E. Sipe, Phys. Rev. B **83**, 195406 (2011).
[33] T. Ando, Y. Zheng, and H. Suzuura, J. Phys. Soc. Jpn. **71**, 1318 (2002).
[34] I. J. Vera-Marun, V. Ranjan, and B. J. van Wees, Phys. Rev. B **84**, 241408 (2011); Nat. Phys. **8**, 313 (2012).
[35] Z. Chen, S. G. Carter, R. Bratschitsch, and S. T. Cundiff, Physica E **42**, 1803 (2010).
[36] E. Ya. Sherman, R. M. Abrarov, and J. E. Sipe, J. Appl. Phys. **104**, 103701(2008).
[37] S. Konschuh, M. Gmitra, D. Kochan, and J. Fabian, Phys. Rev. B **85**, 115423 (2012).